Effect of α-nucleus potential on the ^{27}Al$(\alpha,t)^{28}$Si reaction

S. K. Das,[1] A. S. B. Tariq,[1] A. F. M. M. Rahman,[1] P. K. Roy,[1] M. N. Huda,[1] A. S. Mondal,[1] A. K. Basak,[1] H. M. Sen Gupta,[2] and F. B. Malik[3]

[1]*Department of Physics, University of Rajshahi, Rajshahi, Bangladesh*

[2]*Department of Physics, University of Dhaka, Dhaka, Bangladesh*

[3]*Department of Physics, Southern Illinois University, Carbondale, Illinois 62901*

(Received 15 June 1999; published 16 September 1999)

Full finite-range distorted-wave Born approximation calculations have been performed using molecular, Michel, and normal optical potentials to analyze the angular distributions of cross sections for the 53 transitions populating the bound and unbound states of ^{28}Si via the (α,t) reaction. The parameters of these three potentials have been determined from analyses of the elastic scattering data in the entrance channel at the incident energy involved. The molecular and optical potentials are found to produce satisfactory fits to the data, but the Michel potential seems to be inadequate. For all three potentials in the entrance channel, the deduced l transfers for the transitions to the 15.02, 15.85, and 16.11 MeV states differ from the assignments previously reported. The extracted spectroscopic factors are compared with shell-model predictions. [S0556-2813(99)02510-8]

PACS number(s): 25.55.Ci, 21.10.Jx, 24.10.Eq, 24.50.+g

I. INTRODUCTION

Since the first observation of anomalous large angle scattering (ALAS) by Correlli *et al.* [1] in the elastic scattering of α particles by ^{16}O and ^{32}S, it has also been found to occur in other elastic and nonelastic processes [2–4] induced by α particles. The normal optical-model potentials are found to be consistently inadequate in reproducing ALAS in elastic and inelastic scattering as well as transfer reactions induced by α particles [5–9]. Two alternative types of potential have been proposed to explain ALAS. The first one, advocated by Michel *et al.* [10,11], is a special type of optical potential with a squared Woods-Saxon (WS) geometry. The second one is a molecular type of complex potentials [12–14], having a repulsive core in its real part. Both potentials have been successful in reproducing ALAS in the elastic scattering of α particles [10–15] by some $2s$-$1d$ nuclei. Nonelastic processes have so far been, in most cases, treated within the framework of direct-reaction theory using normal optical potentials in the distorted channels. The anomalies in the data of (α,d) and (α,p) reactions on ^{28}Si [9] have, so far, been analyzed in terms of an incoherent sum of the distorted-wave Born approximation (DWBA) contribution calculated with normal optical potentials and the compound nucleus contribution calculated on the basis of the Hauser-Feshbach model [16]. The method has enjoyed a limited success. In particular, the elastic and transfer data could not be fitted with the same optical potential. To the best of our knowledge there is no available report dealing with the single particle transfer processes using both the molecular- and Michel-type potentials, although these potentials could explain successfully the elastic α-scattering data for a number of $2s$-$1d$ targets [15]. The normal optical model, on the other hand, has failed to explain these data. One may also note that the molecular type of potential has been able reasonably to reproduce [17] the angular distributions of the cross section for the ^{28}Si$(\alpha,p)^{31}$P reaction leading to the ground and excited states. The present study is motivated with a view to test the two potentials in analyzing the one-nucleon transfer reaction on a target, as a part of a series of investigations to find the nature of the α-nucleus interaction which can explain all collision processes involving α-particles including particle transfer reactions. With this objective in mind we have chosen the experimental data of Yasue *et al.* [18] for the ^{27}Al$(\alpha,t)^{28}$Si reaction at $E_\alpha = 64.5$ MeV leading to 56 transitions with an energy resolution of about 35 keV. The DWBA analyses in the work of Yasue *et al.* [18] do not use the appropriate form factor as well as the full finite-range (FFR) calculations for the transitions to states in the unbound region. We have investigated the effect of a FFR using the normal optical, Michel-type, and molecular potentials for particle transfers to bound as well as the unbound states using the resonance form factor, formulated by Vincent and Fortune [19,20]. One may note, however, the lack of reaction data in the analysis at scattering angles greater than about 60° (c.m.) which might be important in determining the details of the potentials. The form of the three types of

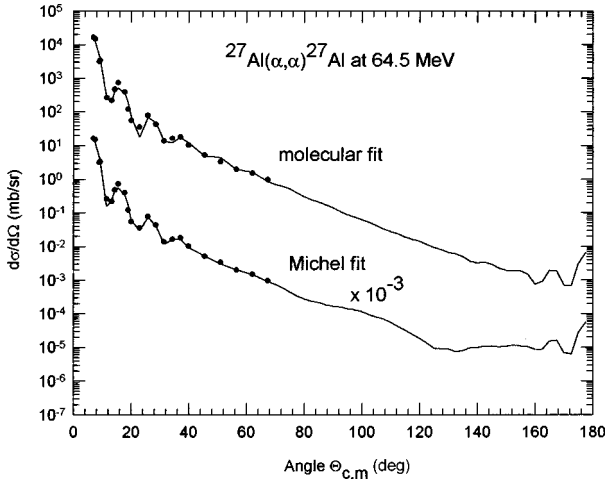

FIG. 1. Fits to the α-^{27}Al elastic scattering data at 64.5 MeV with molecular and Michel potentials. Data are from [18].

TABLE I. Potential Parameters. V adjusted to give the separation energy.

Channel	$\alpha+^{27}$Al			$t+^{28}$Si	$p+^{27}$Al	$t+p$	
				Optical			
Potential type	Optical	Michel	Molecular	set 1	set 2	Bound state	Bound state
V_0 (MeV)	218.0	80.20	52.81	143.82	56.30	V	V
r_0 (fm)	1.24	1.617	1.55	1.19	1.40	1.25	1.25
a_0 (fm)	0.68	0.60	0.57	0.682	0.72	0.70	0.65
V_1 (MeV)			68.46				
R_1 (fm)			2.84				
α		7.40					
ρ (fm)		2.90					
W_0 (MeV)	25.6	55.20	58.13	31.30	50.10		
r_I (fm)	1.24	1.53		1.28	1.40		
a_I (fm)	0.68	0.52		0.999	0.72		
R_w (fm)			3.35				
W_D (MeV)							
r_D (fm)							
a_D (fm)							
$V_{\text{s.o.}}$ (MeV)				4.65		$\lambda=25$	$\lambda=25$
$r_{\text{s.o.}}$ (fm)				0.996			
$a_{\text{s.o.}}$ (fm)				0.280			
r_c (fm)						1.25	1.25
R_c (fm)	5.10	3.90	9.30	3.94	3.94		
	a			b	c	d	d

[a]Reference [34].
[b]Reference [35].
[c]Reference [36].
[d]Reference [27].

α-nucleus potential used in the present work is discussed in Sec. II. Section III gives briefly the salient aspects of the DWBA theory relevant to the present analyses. The DWBA analyses are furnished in Sec. IV. Section V discusses the l transfers involved in populating the various final states, in particular l assignments that differ from the previously reported values [18] for some of the transitions. The conclusions are given in Sec. VI.

II. α-NUCLEUS POTENTIALS

The squared WS Michel potential [10,11] including the Coulomb term $V_c(r)$ is comprised of the following forms [10] of the real $V(r)$ and imaginary $W(r)$ parts:

$$V_M(r) = -V_0\left\{1+\alpha\exp\left[-\left(\frac{r}{\rho}\right)^2\right]\right\} \times\left[1+\exp\left(\frac{r-R_R}{2a_R}\right)\right]^{-2}+V_c(r), \quad (1)$$

$$W_M(r) = -W_0\left[1+\exp\left(\frac{r-R_I}{2a_I}\right)\right]^{-2}, \quad (2)$$

with

$$V_c(r) = \left[\frac{Z_1Z_2e^2}{2R_c}\right]\left[3-\frac{r^2}{R_c^2}\right] \quad (\text{for } r\leqslant R_c) \quad (3)$$

$$= \frac{Z_1Z_2e^2}{r} \quad (\text{for } r>R_c), \quad (4)$$

where $R_C=r_CA_T^{1/3}$ is the Coulomb radius.

This phenomenological form of the potential has been shown to be approximately similar to the equivalent local potential [21] obtained from the microscopic analysis using resonating group method [21,22].

The molecular potential is embedded in the early works of Block and Malik [23] and others [24,25] who recognized this as the manifestation of the role of the Pauli exclusion principle in heavy ion scattering. The potential is obtained from a many body theory utilizing the energy-density functional method [25,26]. This potential has the following forms [14] for the real, $V_m(r)$, and imaginary, $W_m(r)$, parts:

$$V_m(r) = -V_0\left[1+\exp\left(\frac{r-R_0}{a_0}\right)\right]^{-1} + V_1\exp\left[-\left(\frac{r}{R_1}\right)^2\right]+V_c(r), \quad (5)$$

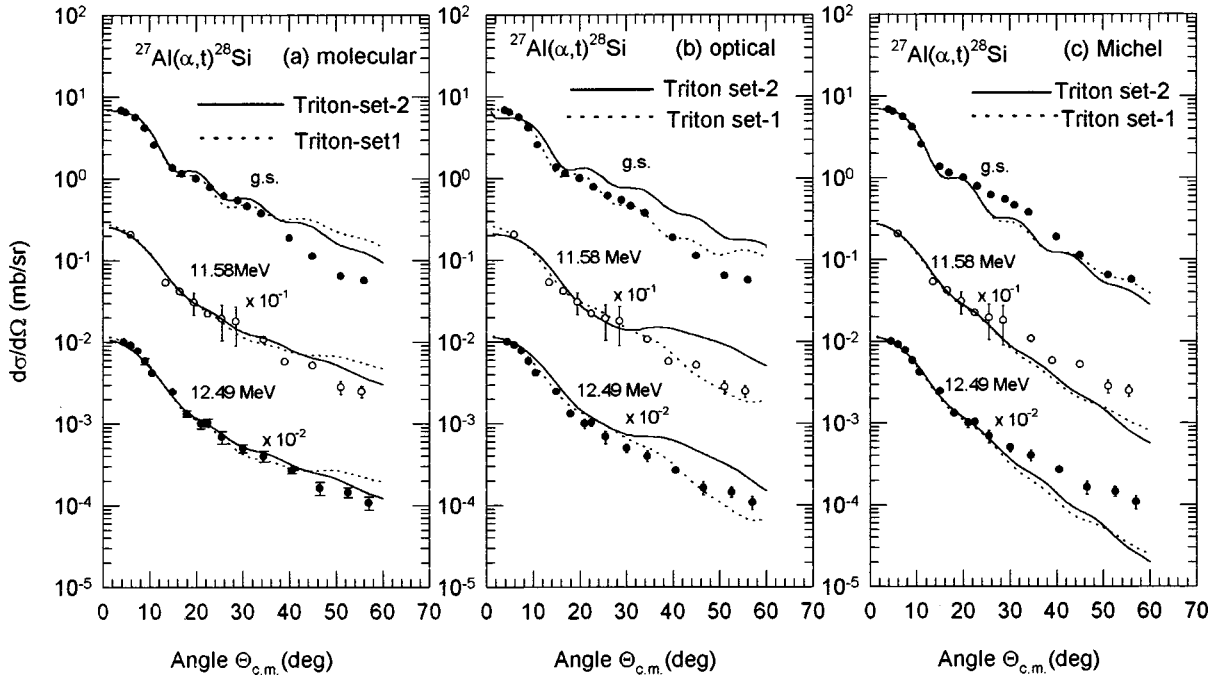

FIG. 2. Full finite-range DWBA predictions compared to data [18] for three transitions using (a) molecular, (b) normal optical, and (c) Michel potentials with set 1 and set 2 (Table I) of triton potentials in the exit channel.

$$W_m(r) = -W_0 \exp\left[-\frac{r}{R_W}\right]^2. \tag{6}$$

Thus the real part is nonmonotonic with a short-range repulsion. The Coulomb radius is scaled [14,15] according to $R_C = R_\alpha + r_C A_T^{1/3}$, R_α being the contribution from α particles.

The normal optical potential for the α-nucleus system including the Coulomb term is given by [27]

$$V(r) = V_c - Vf(x_0) - i\left[Wf(x_W) - 4W_D \frac{d}{dx} f(x_D)\right], \tag{7}$$

where $f(x_i) = (1+e^{x_i})^{-1}$ with $x_i = (r - r_i A^{1/3})/a_i$ and the subscript $i = 0$, W, and D. The Coulomb radius is given by $R_C = r_C A_T^{1/3}$.

III. THEORY OF DWBA FORMALISM

The differential cross section for a transfer reaction with a particular j transfer in the DWBA theory [28] is given by

$$\frac{d\sigma}{d\Omega} = \frac{\mu_i \mu_f}{(2\pi\hbar^2)^2} \frac{k_f}{k_i} \frac{1}{(2J_i+1)(2s_a+1)} \sum |T_{fi}|^2, \tag{8}$$

where J_i and s_a are the spins of the target and the projectile, respectively. μ's and k's are, respectively, the reduced masses and wave numbers. The subscripts i and f refer to the incident and outgoing channels, respectively. Σ denotes the sum over all magnetic substates. T_{fi} is the transition amplitude, having the form

$$T_{fi} = J \int d^3\mathbf{r}_a \int d^3\mathbf{r}_b \chi_f^{(-)*}(\mathbf{k}_b, \mathbf{r}_b) V_{fi}(\mathbf{r}) \chi_i^{(+)}(\mathbf{k}_a, \mathbf{r}_a). \tag{9}$$

Here J is the Jacobian of the transformation to the relative coordinates. $\chi_i^{(+)}$ and $\chi_f^{(-)}$ are the distorted waves in the initial and final channels, respectively, with outgoing and incoming boundary conditions. $\mathbf{r}_a$ and $\mathbf{r}_b$ are the coordinates of the outgoing and incoming particles a and b relative to the center of mass of the system. $\mathbf{k}_a$ and $\mathbf{k}_b$ are the momenta of the projectile and ejectile, respectively. The distorted waves $\chi(\mathbf{k},\mathbf{r})$ are generated from the Schrödinger equation [28]

$$\left\{\nabla^2 + k^2 - \left(\frac{2\mu}{\hbar^2}\right)[V(r) + V_c(r)]\right\} \chi(\mathbf{k},\mathbf{r}) = 0, \tag{10}$$

where $V(r)$ is the distorting potential and μ is the reduced mass of the pair. The distorting potential may be the normal optical, Michel, or molecular potential. The V_{fi} is the transition matrix having the form [28]

$$V_{fi} = \langle \psi_f \psi_b | V | \psi_i \psi_a \rangle. \tag{11}$$

Equation (11) can be, under certain circumstances, factored into (i) the overlap integral $\langle \psi_f | \psi_i \rangle$ containing the spectroscopic amplitude and the information on the nuclear struc-

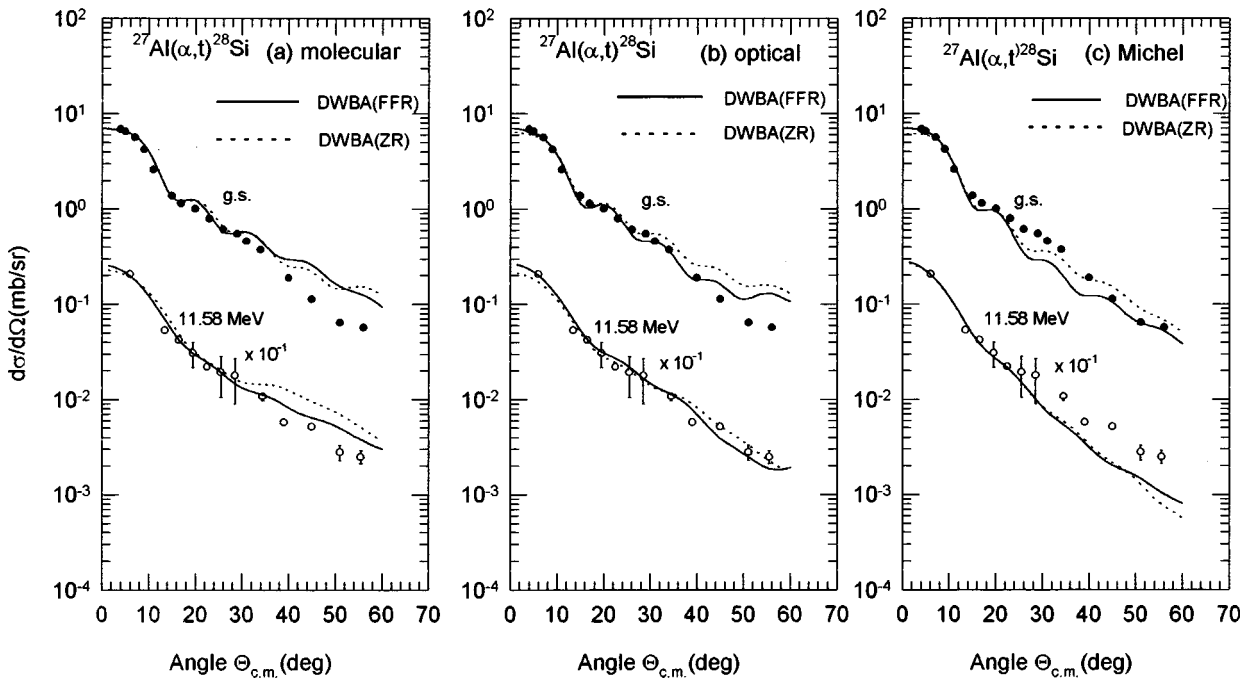

FIG. 3. Full finite-range (solid curves) and zero-range (dotted curves) DWBA predictions using (a) molecular, (b) normal optical, and (c) Michel potentials for the g.s. and $E_x = 11.58$ MeV transitions are compared to data. Data are from [18].

ture and (ii) the effective interaction $\langle \psi_a | V | \psi_b \rangle$ responsible for the transition from the initial channel to the final channel [28]. In the analysis of single nucleon stripping reactions, it is assumed that the transferred nucleon is picked up from the projectile and deposited into a shell-model state of the final nucleus. Thus the DWBA calculations in the present analysis involve the single particle proton wave function in the final nucleus as well as that in the incident α particle.

In the isospin representation, Eq. (8) can be reduced into a more tractable form for the calculation of the cross section of the stripping reaction in FFR calculations [30]:

$$\left(\frac{d\sigma}{d\Omega}\right)_{\text{expt}} = \frac{2J_f+1}{2J_i+1} C^2 S s \left(\frac{d\sigma}{d\Omega}\right)_{\text{DWUCK5}}. \tag{12}$$

$(d\sigma/d\Omega)_{\text{DWUCK5}}$ means the cross section calculated with the computer code DWUCK5, C^2 is the isospin Clebsch-Gordon coefficient, and S and s are, respectively, the heavy and light particle spectroscopic factors. J_f and J_i are the total spins of the final and initial nuclei, respectively. The corresponding expression [30] for a zero-range (ZR) approximation is

$$\left(\frac{d\sigma}{d\Omega}\right)_{\text{expt}} = \frac{(2J_f+1)}{(2J_i+1)(2j+1)} D_0^2 C^2 S \left(\frac{d\sigma}{d\Omega}\right)_{\text{DWUCK4}}. \tag{13}$$

D_0^2 is the normalization constant, and $(d\sigma/d\Omega)_{\text{DWUCK4}}$ is the cross section calculated with DWUCK4.

For the analyses of the data for the unbound states of the final nucleus, the resonance form factor formulated by Vincent and Fortune [19,20] is applied. It is assumed that the resonance has a Breit-Wigner shape, and in such a case the differential cross section is given [20] by

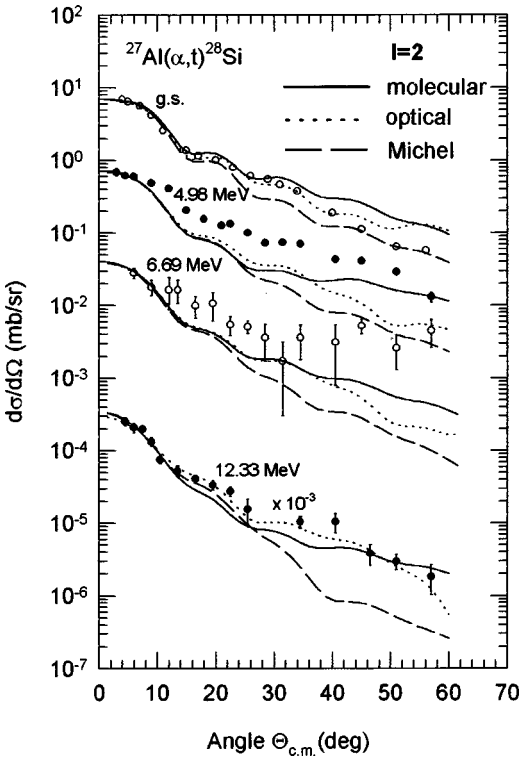

FIG. 4. Full finite-range DWBA predictions using molecular (solid curves), normal optical (dotted curves), and Michel (dashed curves) potentials for the transitions with l values indicated are compared to data (solid or open circles). The triton potential of set 1 has been used with the normal optical and Michel potentials, and that of set 2 with the molecular potential in the α channel. Data are from [18].

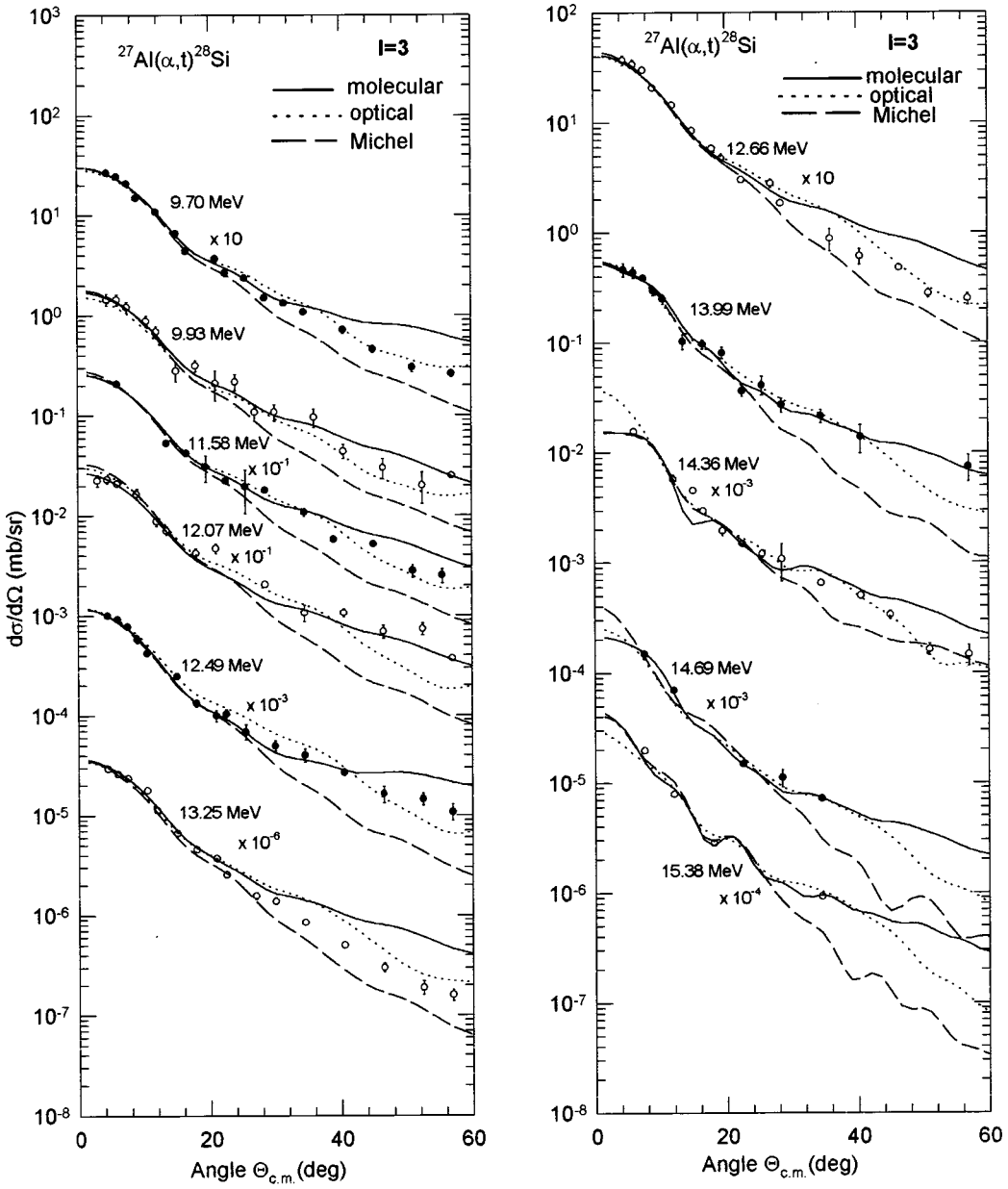

FIG. 5. Same as in Fig. 4.

$$\frac{d\sigma}{d\Omega}=\frac{\Gamma\mu k}{\hbar}\frac{d\sigma^F}{d\Omega}. \tag{14}$$

Here $d\sigma^F/d\Omega$ is the cross section predicted at the energy of resonance (the positive energy of the transferred proton relative to the core). Γ is the width of the resonance, μ is the reduced mass of the transferred proton and the target nucleus, and k is the wave number of the proton at the resonance energy. Γ is estimated from the relation [20]

$$\frac{2}{\Gamma}=\frac{2\mu}{\hbar^2 k}\left[\int_0^{R_{\max}}|u(r)|^2dr+\frac{G}{2k}\frac{d}{dk}\left(\frac{G'}{G}\right)\right]. \tag{15}$$

Here $u(r)$ is the radial wave function of proton in the field of target core and $r=R_{\max}$ is the distance beyond which nuclear potentials are assumed to be zero. G and G' are the irregular Coulomb function and its derivative at $r=R_{\max}$, respectively.

IV. DWBA ANALYSIS

The ZR and FFR DWBA calculations for the angular distributions have been performed using the computer codes DWUCK4 and DWUCK5 [30], respectively. Both codes are modified to include Michel and molecular potentials. For the ZR calculations, a Gaussian form of finite-range correction in the local energy approximation [29,30] with the correction parameter $R=0.7$ fm has been used. Corrections due to the nonlocality [30,31] of potentials in the conventional form have been applied using the nonlocality parameters $\beta(\alpha)=0.2$ and $\beta(p)=0.85$ fm. The FFR analyses have been performed for both bound and unbound regions

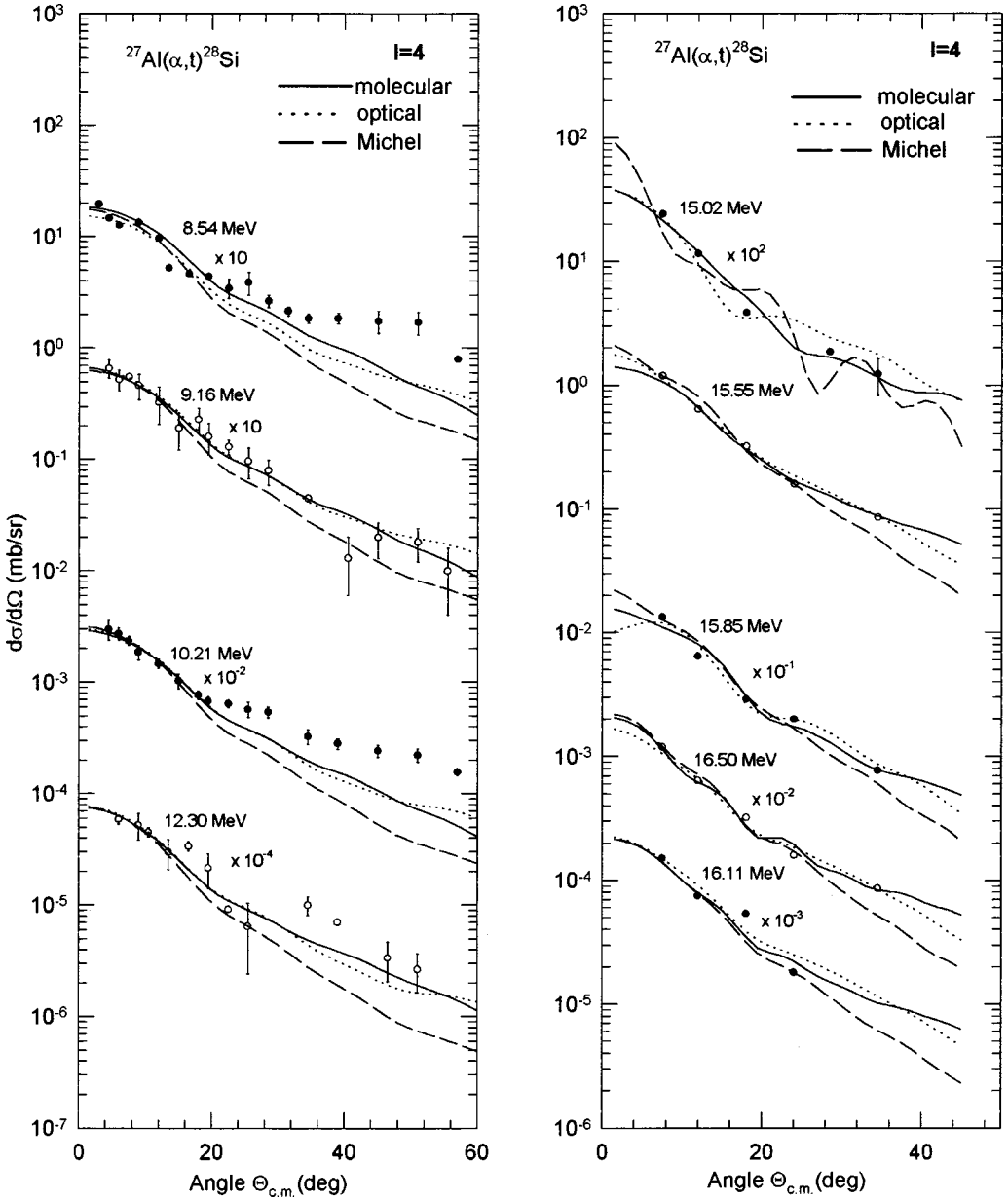

FIG. 6. Same as in Fig. 4.

using the Michel, molecular, and normal optical model types of potentials.

A. Choice of potential parameters

For the entrance channel, the parameters of the molecular and Michel types of potential are generated by fitting the angular distributions of elastic data [18] using the chi-squared minimization code MINUIT [32] in conjunction with the optical-model code SCAT2 [33] modified to incorporate the Michel and molecular potentials. The fits to the elastic data are shown in Fig. 1. The normal optical-potential-parameter set used in the present analysis is taken from [34]. The parameters of all three types of potentials are given in Table I. The bound state geometry parameters are also noted in Table I. For a bound state of ^{28}Si for both the FFR and ZR calculations, as well as for the bound state of the α for the FFR calculations, the single proton transfer wave function has been computed adjusting the WS potential well depth so that its eigenvalue equals the separation energy [29].

For the triton potential in the exit channel, different sets of triton potentials have been tried. Two sets of triton potentials, labeled set 1 and set 2 in Table I, have been found to fit the data reasonably well with the molecular, normal optical, or Michel potential in the entrance channel as can be seen in Figs. 2(a)–2(c). Set 2 of triton potentials produces a slightly better fit at the larger scattering angle region when the molecular potential is employed in the α channel [Fig. 2(a)]. On the other hand, the normal optical potential in the α channel produces a good fit to the data for set 1 of triton potentials in the exit channel [Fig. 2(b)]. We have, therefore, finally chosen set 2 of triton potentials with the molecular potential and

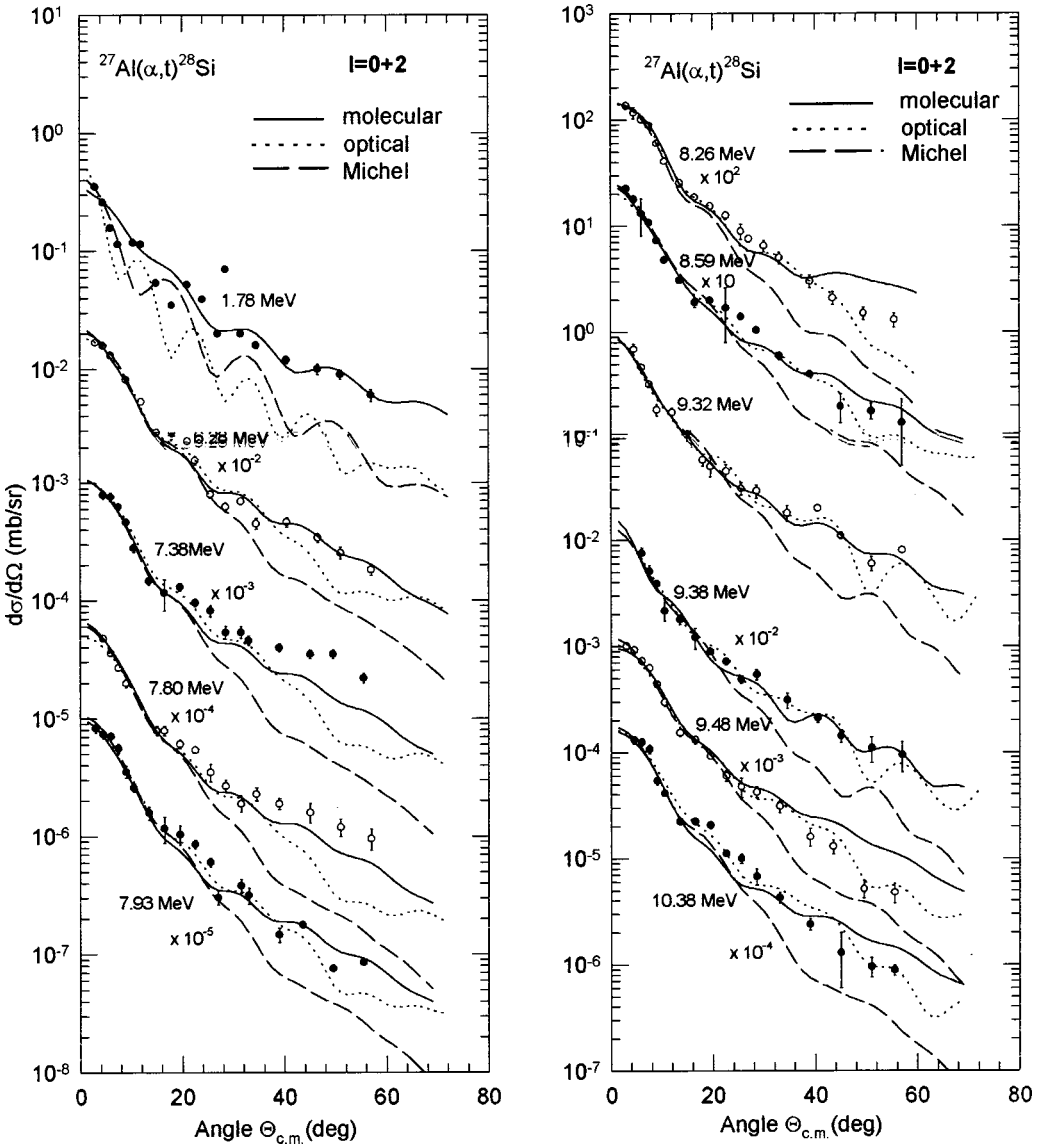

FIG. 7. Incoherent sums of full finite-range DWBA predictions using molecular (solid curves), normal optical (dotted curves), and Michel (dashed curves) potentials for the transitions with l values indicated are compared to data (filled or open circles). Data are from [18].

set 1 of the triton potentials with the Michel or normal optical potential in the α channel for the analyses of the data. It is to be noted that the sensitivity of the predicted cross sections to the triton potential seems to be much stronger in the case of the normal optical potential in the entrance [Fig. 2(b)] than for cases with the other two potentials.

B. Angular distributions

The comparison of the ZR and FFR DWBA calculations of the angular distributions for the ground state (g.s.) and the state at the excitation energy $E_x = 11.58$ MeV using the molecular, Michel, and normal optical potentials for the best fits to the experimental data are shown in Figs. 3(a)–3(c).

The FFR DWBA calculations for angular distributions for the best fits to the data using all three types of α-nucleus potentials for various l transfers are compared to the experimental data in Figs. 4–9 for all levels. The levels in Figs. 4–9 are grouped according to the associated l transfers. The levels populated through the $l=2$, 3, and 4 transfers are shown in Figs. 4–6, respectively. On the other hand, the levels which have been obtained through the incoherent sum of more than one l transfer such as $l=0+2$, $1+3$, and $2+4$ are shown, respectively, in Figs. 7–9. The DWBA fit to the unresolved group at $E_x = 6.88$ MeV is also shown in Fig. 8 with the total incoherent contribution from $l=2+3$. In the previous study, Yasue *et al.* associated an $l=3$ transfer for fitting 15.02, 15.85, and 16.11 MeV transitions, but in the present study, it seems to be $l=4$. The predicted angular distributions using each of the molecular, Michel, and normal optical potentials for both l transfers ($l=3$ and $l=4$) are compared to the data in Fig. 10. Clearly, the $l=4$ transfer is preferred in all three cases.

C. Spectroscopic strengths

The spectroscopic strengths of a reaction for a transition to a final state $(J_f;T_f)$ with the transferred configuration (lj) is related to the spectroscopic factor S_{lj} [38] by

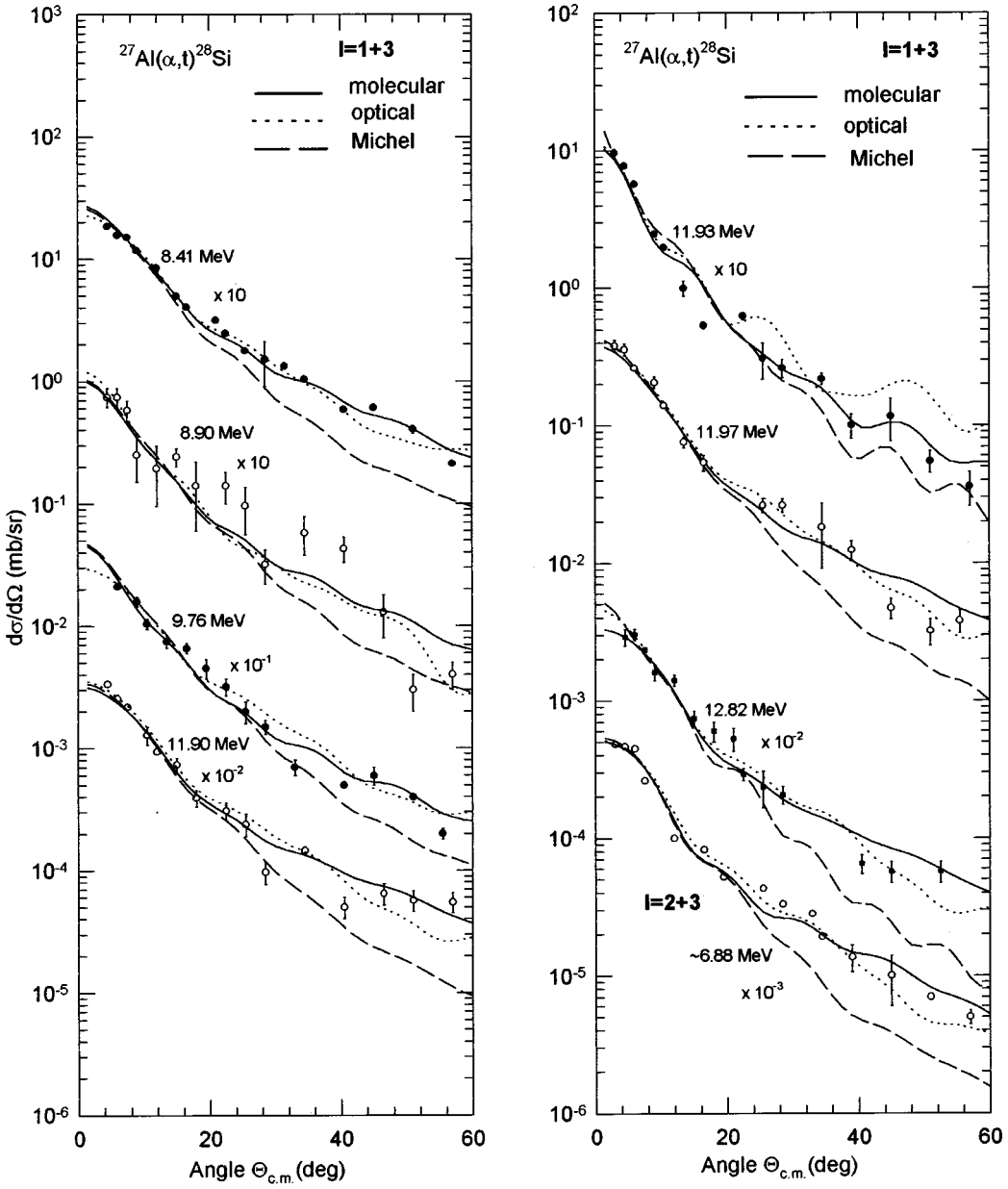

FIG. 8. Same as in Fig. 7. The data of the 6.88 MeV transition are compared to the $l=2+3$ DWBA predictions.

$$G_{lj}=\frac{(2J_f+1)}{(2J_i+1)}C^2S_{lj}, \tag{16}$$

where C is the Clebsch-Gordon coefficient involving isospins of the target and the final nucleus.

The sum rule for the spectroscopic strength in the case of the ^{27}Al$(\alpha,t)^{28}$Si reaction can then be expressed [38] by

$$\sum_{J_f} G_{lj}=\frac{1}{2}\langle n \text{ holes}\rangle \quad (\text{for } T_f=1)$$

$$=\frac{1}{2}\langle p \text{ holes}\rangle-\frac{1}{2}\langle n \text{ holes}\rangle \quad (\text{for } T_f=0),$$

where $\langle p$ holes$\rangle$ and $\langle n$ holes$\rangle$ are, respectively, the effective number of proton holes and neutron holes in the orbit (lj).

The total strength comprising transitions with $T_f=0$ and 1 is then

$$\sum_{J_f,T_f} G_{lj}=\langle p \text{ holes}\rangle. \tag{17}$$

The deduced sum of strengths for all $l=2$ transitions with $j=3/2,5/2$ transfers and $T_f=0,1$ is $\Sigma G=2.33$. This is almost half of the sum rule strength 5.0, the number of proton holes in the $1d_{5/2}$ and $1d_{3/2}$ orbits. Similarly, the sum of all $l=0$ transition strengths for both $T_f=0$ and 1 has been found to be $\Sigma G=0.96$, which is again 50% of the expected sum of 2.0.

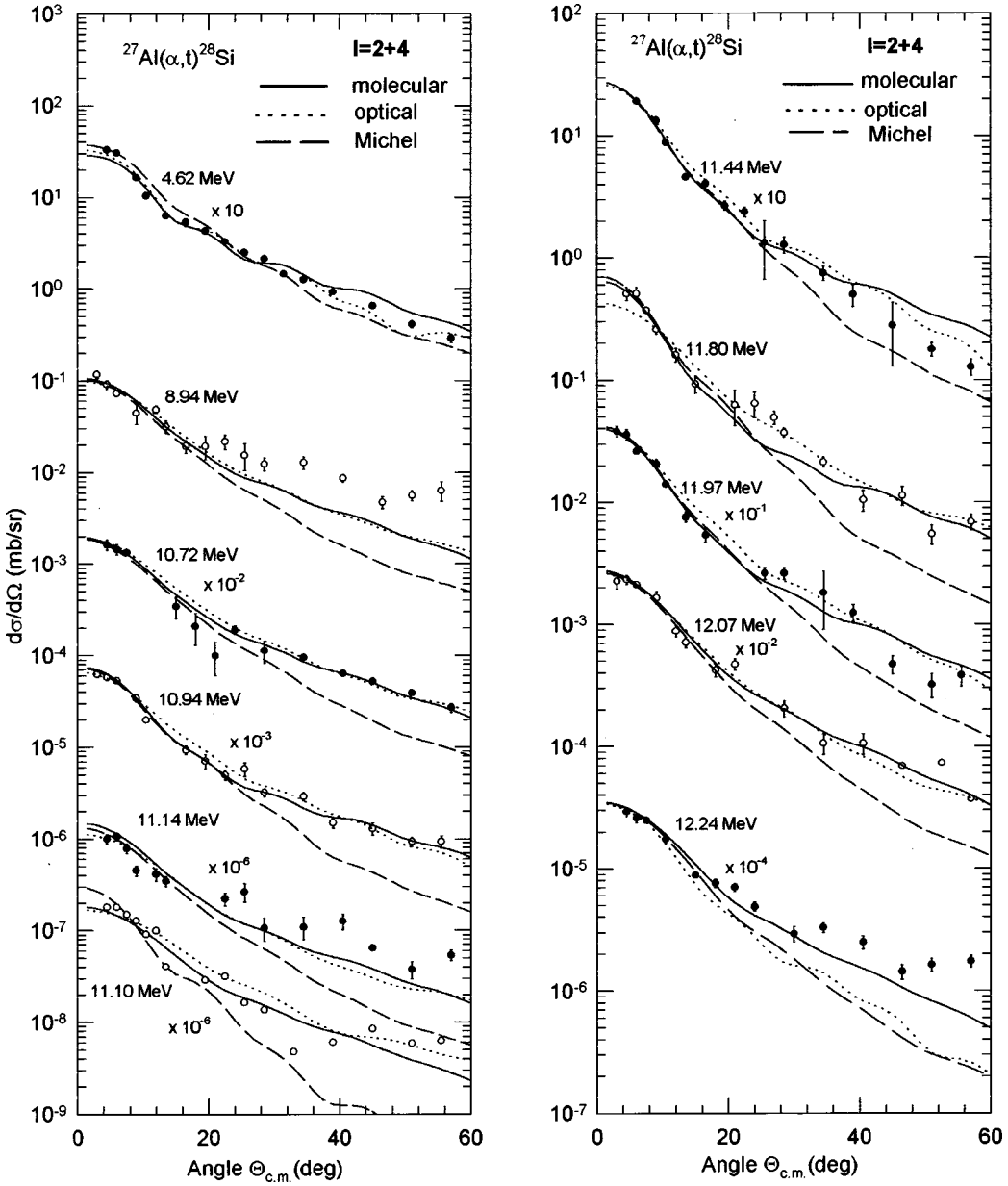

FIG. 9. Same as in Fig. 7.

The extracted transition strengths for the $(6^-;0)$ state at $E_x=11.58$ MeV and $(6^-;1)$ state at $E_x=14.36$ MeV, which have the stretched configuration $(1d_{5/2}{}^{-1},1f_{7/2})$ in the shell model, are 0.14 and 0.23, respectively, which is small compared to the expected full strength of 1.08 for each. If one considers, however, the fragmentation of 6^- strengths as due to the deformed structure of the ^{28}Si core, using the assumptions that (i) the vibrational state of the core does not change in the transition, (ii) the core has negative deformation, and (iii) the proton-hole configuration in the target is $|j_i=5/2, \Omega_i=1/2\rangle$—i.e., the target has $J_i=5/2$ and $K_i=1/2$—one may calculate the spectroscopic strength due to deformation using the expression [39,40]

$$G=\frac{(2J_f+1)}{(2J_i+1)}C^2S=g^2C^2\langle J_iK_ij\Omega|J_fK_f\rangle^2C_{Nlj}(\Omega\omega\alpha)^2, \tag{18}$$

where $C_{Nlj}(\Omega\omega\alpha)$ as defined in [39,40] are the coefficients connecting a deformed single particle state to spherical eigenstates, and g^2 is unity as $K_i\neq 0$. The values of these coefficients have been taken from [41]. Equation (18) with $K_f=4$ results in a strength of $G=0.083$ for each of the $(6^-;0)$ and $(6^-;1)$ states, which is, indeed, small.

V. DISCUSSION

In the present study, 53 transitions have been analyzed with all three types of potentials. The analyses involve (i) 4 transitions with the $l=2$ transfers (Fig. 4), leading to the ground, 4.98, and 6.69 MeV states with the unique $j=5/2$ transfer and the 12.33 MeV state which is assumed to be populated via $j=3/2$, (ii) 11 transitions with $l=3$ (Fig. 5), (iii) 9 transitions with $l=4$ (Fig. 6), (iv) 11 transitions with

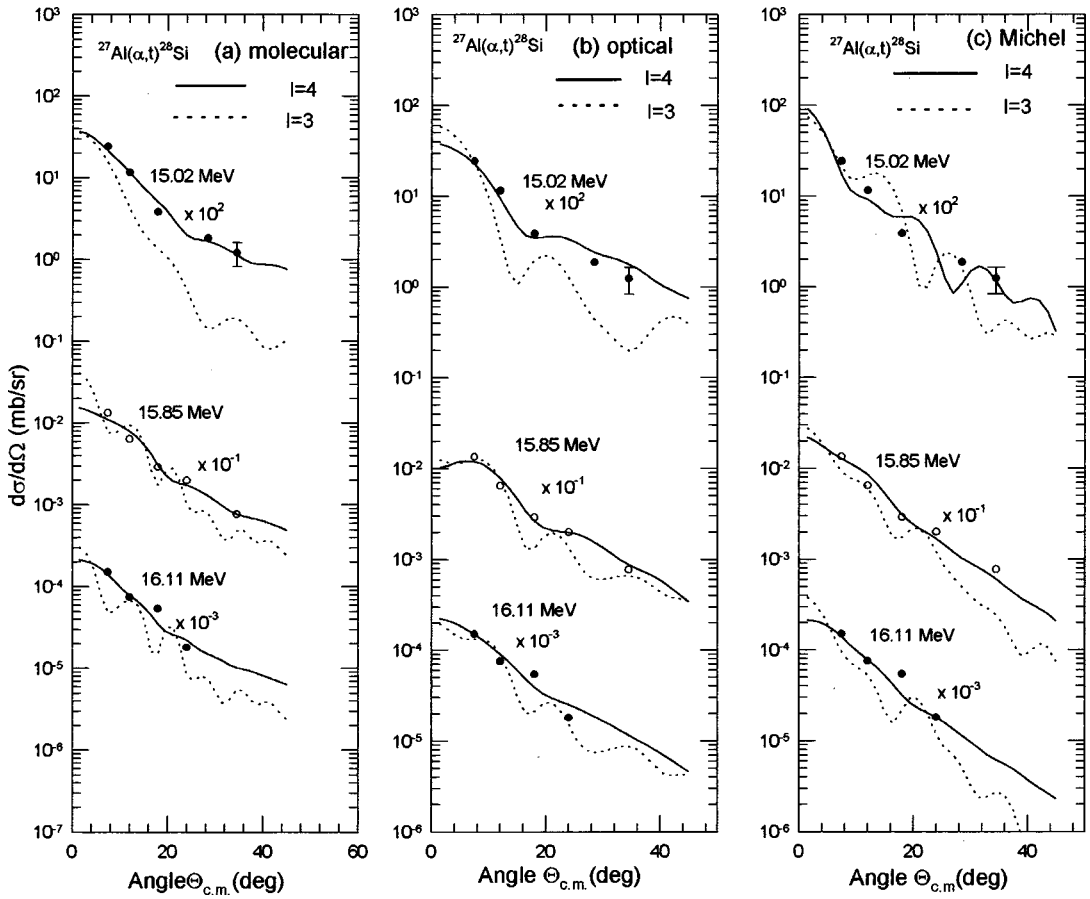

FIG. 10. Full finite-range DWBA predictions for transitions with $l=4$ (solid curves) and $l=3$ (dotted curves) values are compared to data for three transitions using (a) molecular, (b) normal optical, and (c) Michel potentials. Data are from [18].

the admixture $l=0+2$ (Fig. 7), (v) 7 transitions with the admixture $l=1+3$ (Fig. 8), (vi) 1 transition with $l=2+3$ (Fig. 8) populating probably two unresolved states with opposite parities at about $E_x=6.88$ MeV, and (vii) 11 transitions with the admixture $l=2+4$ (Fig. 9) transfer. The data of the transition to the 11.97 MeV state are compared to the DWBA predictions twice, once in Fig. 8 for the $l=1+3$ transfer and again in Fig. 9 for the $l=2+4$ transfer as both transfers produce acceptable fits to the data.

In Fig. 3 the FFR and ZR calculations are compared to the angular distribution data for transitions to the g.s. and the state at $E_x=11.58$ MeV. The improvement of the fits due to predictions of the former over those of the latter underlines the importance of the FFR calculations.

It is evident from Figs. 4–9 that the full finite-range DWBA analyses using the molecular and normal optical potentials fits quite satisfactorily the experimental data of the 44 transitions out of 53 with 9 other states fitted moderately. In general, the fits with the molecular and normal optical potentials seem to be of the same quality, but the fits with the Michel potential are comparatively poor. At forward scattering angles $<20°$ or so, all three potentials yield, to some extent, the same results. But at larger scattering angles, for the bound state transitions with excitation energies up to 11.58 MeV, the molecular potential provides a better fit, although the normal optical potential competes reasonably well, while the Michel potential fails completely. For the continuum states with excitation energies above 11.58 MeV both molecular and normal optical potentials yield again comparable results with quite reasonable fits to the data, but the Michel potential fails again. At reaction angles larger than 30°, the difference in the predictions due to the three distorting α-nucleus potentials becomes very prominent and increases with the reaction angle. It is also to be mentioned that for some transitions, e.g., the 4.98, 6.69, 8.54, 10.21, and 12.24 MeV states, neither of the three types of potentials could produce good fits to the angular distributions, indicating probably that reaction mechanisms other than the direct one may be involved in these cases.

Yasue *et al.* [18] reported that an admixture of $l=1$, 2, and 3 was needed to fit the data of the level 6.88 and 6.89 MeV, but in the present study an admixture of $l=2$ and 3 suffices to fit satisfactorily the angular distributions of these unresolved levels (Fig. 8). Furthermore, they [18] used the $l=0+2+4$ admixture for the 7.93 and 8.26 MeV transitions, while in the present work $l=0+2$ seems to be sufficient to fit the data quite well (Fig. 7). Moreover, as mentioned earlier, Yasue *et al.* [18] associated the 15.02, 15.85, and 16.11 MeV transitions with the $l=3$ transfer, but the comparison of the predictions in the present analyses for $l=3$ and 4 in Fig. 10 for each of the three potentials shows that the angular distributions for these transitions are better

TABLE II. States of ^{28}Si observed in the ^{27}Al(α,t) reaction at $E_\alpha = 64.5$ MeV.

			$(2J_f+1)C^2Ss$[a] Present work			
E_x (MeV)	$J^\pi;T$ b	$l(nlj)$	c	d	e	f,g
g.s	$0^+;0$	$2(0d_{5/2})$	4.8	4.5	4.5	4.6
1.78	$2^+;0$	$(0+2)$	0.7, 1.08	0.84, 1.26	0.672, 1.008	1.7, 1.2
4.62	$4^+;0$	$(2+4)$	2.13, 0.022	2.90, 0.396	2.22, 0.117	2.5, 0.04
4.98	$0^+;0$	$2(0d_{5/2})$	0.42	0.6	0.75	0.48
6.28	$3^+;0$	$(0+2)$	0.138, 1.24	0.36, 2.04	0.63, 1.47	0.39, 1.4
6.69	$0^+;0$	$2(0d_{5/2})$	0.03	0.048	0.048	0.04
6.88	$3^-;0$	$(2+3)$	0.27, 0.03	0.57, 0.03	0.456, 0.024	0.65, 1.1, 2.6
6.89	$4^+;0$					
7.38	$2^+;0$	$(0+2)$	0.06, 0.86	0.3, 1.2	0.276, 1.104	0.15, 0.90
7.42	$2^+;0$					
7.80	$3^+;0$	$(0+2)$	0.26, 0.396	0.357, 0.663	0.315, 0.585	0.22, 0.35
7.93	$2^+;0$	$(0+2)$	0.27, 0.672	0.63, 1.17	0.441, 0.819	0.7, 0.65, 0.06
8.26	$2^+;0$	$(0+2)$	0.30, 1.20	0.15, 1.65	0.38, 1.5	0.13, 1.1
8.41	$4^-;0$	$(1+3)$	0.48, 0.72	0.9, 0.9	0.9, 0.9	0.45, 1.0
8.54	$6^+;0$	4	0.48	0.78	0.9	0.13
8.59	$3^+;0$	$(0+2)$	1.0, 1.51	2.85, 2.85	1.8, 1.8	0.8, 1.9
8.90	$1^-;0$	$(1+3)$	0.048, 0.072	0.076, 0.032	0.055, 0.023	0.018, 0.048
8.94	$4^+;0$	$(2+4)$	0.054, 0.023	0.022, 0.086	0.022, 0.086	0.11, 0.06
	$5^-;0$	or 3	0.054	0.066	0.036	0.06
9.16	$4^+;0$	4	0.02	0.03	0.03	0.06
9.32	$3^+;1$	$(0+2)$	1.176, 0.50	1.95, 1.05	1.365, 0.735	1.5, 0.49
9.38	$2^+;1$	$(0+2)$	1.33, 0.88	3.36, 1.44	3.84, 0.96	1.6, 1.0
9.48	$2^+;0$	$(0+2)$	0.52, 0.90	1.5, 1.5	1.026, 0.054	0.2, 0.24
9.70	$5^-;0$	3	1.20	1.8	1.8	1.8
9.76	$(2,3)^-;0$	$(1+3)$	0.038, 0.113	0.576, 0.144	0.385, .096	0.06, 0.17
9.93	$(1,2)^-;0$	3	0.60	1.17	0.99	0.11
10.21	$(2-4)^+;0$	4	0.096	0.126	0.126	0.17
10.38	$3^+;1$	$(0+2)$	0.66, 1.98	1.13, 3.38	0.75, 2.25	0.65, 2.3
10.72	$1^+;0+1$	$(2+4)$	0.113, 0.038	1.92, 0.48	0.144, 0.036	0.11, 0.009
10.94	$+$	$(2+4)$	0.70, 0.08	1.37, 0.072	1.083, 0.057	0.32
11.10		$(2+4)$	0.105, 0.045	0.108, 0.072	0.072, 0.048	0.1, 0.04,
11.14	2^+	$(2+4)$	0.363, 0.297	0.274, 0.068	0.168, 0.042	0.02, 0.06
11.44	$2^+,3^+,4^+;(0,1)$	$(2+4)$	2.96, 0.16	5.99, 0.315	3.99, 0.21	3.8, 0.39
11.45	$1^+;1$					
11.58	$6^-;0$	3	1.41	1.86	1.68	2.1
11.80	$+$	$2+4$	0.19, 0.157	0.36, 0.36	0.5, 0.22	0.13, 0.12
11.90	$3^-;0$	$(1+3)$	0.4, 0.08	0.126, 0.294	0.099, 0.231	0.49, 0.17
11.93	$-$	$1+3$	3.70, 0.195	5.67, 0.63	4.28, 0.23	4.7
11.97	$(2^+,4^+);0$	$2+4$	0.59, 0.066	0.972, 0.108	0.11, 0.066	0.5, 0.09
	or $3^-;0$	or $1+3$	0.41, 0.221	0.655, 0.353	0.43, 0.23	0.4, 0.3
12.07	$(2^\pm);0$	$2+4$	0.21, 0.09	0.315, 0.135	0.252, 0.108	0.3, 0.09
		or 3	0.21	0.36	0.24	0.2
12.24	$3^++4^+;0$	$2+4$	0.1, 0.06	0.144, 0.216	0.144, 0.216	0.27, 0.12
12.30	$2^+;0$	4	0.39	0.51	0.51	0.06
12.33	$1^+;1$	2	0.72	1.32	0.9	0.55
12.49	$3^-;0$	3	0.84	1.2	1.14	1.0
12.66	$4^-;1$	3	3.00	5.4	4.2	3.8
12.82	$1^-;0$	$1+3$	0.14, 0.32	0.20, 0.46	0.15, 0.36	0.03, 0.32
13.25	$5^-;1$	3	3.30	5.4	4.2	3.6

TABLE II. *(Continued).*

			$(2J_f+1)C^2Ss$[a] Present work			
E_x (MeV)	$J^\pi;T$ b	$l(nlj)$	c	d	e	f,g
13.99	−	3	0.63	1.02	0.78	1.6
14.36	$6^-;1$	3	2.40	2.88	2.7	3.7
14.69	−	3	0.24	0.51	0.33	0.39
15.02	−	4	0.15	0.21	0.21	0.70
15.38	−	3	0.45	0.78	0.57	0.55
15.55	+	4	0.12	0.21	0.15	0.09
15.85	−	4	0.11	0.222	0.156	0.36
16.11	−	4	0.48	0.24	0.48	0.41
16.50	+	4	0.14	0.24	0.18	0.07

[a]$s=2.0$ is the light particle spectroscopic factor.
[b]Reference [37].
[c]Optical.
[d]Michel.
[e]Molecular.
[f]Reference [18].
[g]Light particle spectroscopic factor is not mentioned in [18].

fitted by the $l=4$ transfer. It is also obvious from Fig. 10 that the predictions with the molecular potential bring out the difference more distinctly in the angular patterns for $l=3$ and $l=4$.

The spectroscopic factors (Table II) extracted using the molecular potential are comparable to those obtained using the normal optical potential, but are a bit larger for some cases. In general, those deduced from using the Michel potential are even larger. Considering the quality of the fits, the spectroscopic factors obtained with the Michel potential are expected to be less reliable.

The spectroscopic strengths extracted from the use of the molecular potential are compared to those calculated from the shell model [42] in Table III. The predicted and deduced strengths agree for most of the $l=2$ transitions except that for the 6.89 MeV state. The extracted strengths for the $l=0$ transitions to the 1.78, 6.28, and 9.32 MeV state are much weaker than the predicted values. This may be partly ascribed to the fact that the matching l transfer $|k_iR_i - k_fR_f|$ (k's and R's are, respectively, the momenta and interaction distances in the reaction channels) lies in the range 2–4 over $E_x=0.0-14.36$ MeV of the final nucleus and hence $l=0$ is a mismatched transfer. The $l=0$ shell-model wave functions used in [42] may not be good due to truncation.

The extracted sum of strengths for all $l=2$ as well as for all $l=0$ transitions has a factor of 2 missing from the expected magnitude, e.g., the effective number of proton holes in the transfer orbits. This is surprising when one considers that the states of ^{28}Si resulting from the $j^\pi=1/2^+$, $3/2^+$, $5/2^+$ transfers in the reaction are highly improbable to exist at $E_x>16.50$ MeV. The spherical shell model cannot probably take up the whole of the transition strength, and some of the strength drains off as a result of deformation. For the transition to each of the 6^- states at $E_x=11.58$ and 14.36

TABLE III. Comparison of the deduced spectroscopic strengths to the shell-model predictions.

			$G=\frac{(2J_f+1)}{(2J_i+1)}C^2S$	
E_x (MeV)	$J^\pi;T$ a	$l(nlj)$	Present work[b]	Shell model[c]
g.s.	$0^+;0$	$2(0d_{5/2})$	0.375	0.53
1.78	$2^+;0$	$(0+2)$	0.06, 0.08	0.38, 0.06
4.62	$4^+;0$	$(2+4)$	0.19, 0.01	0.33, 0.00
4.98	$0^+;0$	$2(0d_{5/2})$	0.06	0.05
6.28	$3^+;0$	$(0+2)$	0.05, 0.12	0.34, 0.14
6.69	$0^+;0$	$2(0d_{5/2})$	0.004	0.005
6.88	$3^-;0$	3	0.002	0.0
6.89	$4^+;0$	2	0.038	0.27
7.38	$2^+;0$	$(0+2)$	0.02, 0.09	0.02, 0.17
7.42	$2^+;0$			
7.80	$3^+;0$	$(0+2)$	0.03, 0.05	0.357, 0.663
7.93	$2^+;0$	$(0+2)$	0.04, 0.07	0.00, 0.13
8.59	$3^+;0$	$(0+2)$	0.15, 0.15	0.035, 0.21
9.32	$3^+;1$	$(0+2)$	0.11, 0.06	0.38, 0.06
9.38	$2^+;1$	$(0+2)$	0.32, 0.08	0.23, 0.05
10.38	$3^+;1$	$(0+2)$	0.06, 0.19	0.01, 0.20
10.72	$1^+;0+1$	$(2+4)$	0.012, 0.006	0.015, 0.00
11.58	$6^-;0$	3	0.14	0.083[d]
14.36	$6^-;1$	3	0.23	0.083[d]

[a]Reference [37].
[b]Molecular potential.
[c]Reference [42].
[d]Deformed shell model [39,40].

MeV, the predicted strength $G = 0.083$, calculated on the basis of deformed shell model [39,40], is not adequate enough to explain the observed values (Table III). The band mixing effects due to Coriolis coupling [43] may have significant effects on these transition strengths and is worth further investigation.

VI. CONCLUSIONS

In the present work, both the molecular and Michel types of α-nucleus potential producing the same quality fit to the α-^{27}Al elastic data have been used to analyze one-nucleon transfer data to the bound and unbound states of ^{28}Si. The present work shows that full finite-range DWBA analyses with the molecular potential can describe the angular distributions of the transitions to the bound and unbound states in ^{28}Si at least as satisfactorily, if not somewhat better, as those obtained using the normal optical potential. On the other hand, the Michel potential is, in general, inadequate to explain the data. Furthermore, at reaction angles greater than about 30°, the DWBA calculations using the three types of α-nucleus potentials become significantly different and, hence, the experimental data at larger angles appear to be essential to decide the nature of the α-nucleus potential. To determine the parameters of the potential more accurately, elastic scattering data at large angles would also be helpful.

ACKNOWLEDGMENTS

This work is partially supported by Grant No. INT-9808892 of the U.S. National Science Foundation and a grant from Rajshahi University. The authors thankfully acknowledge the grants. The authors are also thankful to Professor P. D. Kunz of the University of Colorado for making the codes DWUCK4 and DWUCK5 available to us. One of us, S.K.D. is thankful to Shahjalal University of Science and Technology, Bangladesh, for the study leave grant and to the American Institute for Bangladesh Studies for a travel grant to the U.S.

[1] J. C. Correlli, E. Bleuler, and J. Tandem, Phys. Rev. **116**, 1184 (1959).
[2] H. Oeschler, H. Schroter, H. Ficjs, L. Baum, G. Gaul, H. Ludechi, R. Santo, and R. Stock, Phys. Rev. Lett. **28**, 694 (1972).
[3] Å. Bredbacka, M. Brenner, K. M. Källman, P. Manngård, Z. Máté, S. Szilágyi, and L. Zolnai, Nucl. Phys. **A574**, 397 (1994).
[4] L. Jarczyk, B. Maciuk, M. Siemaszko, and W. Zipper, Acta Phys. Pol. B **7**, 531 (1976).
[5] H. Kitazawa, Y. Harima, and N. Mukai, Nucl. Phys. **A510**, 429 (1990).
[6] B. Xiumin, L. Shiming, W. Yuanda, Y. Rongfang, H. Bingyin, and S. Zuxun, Chin. Phys. **6**, 645 (1986).
[7] A. W. Obst and K. W. Kemper, Phys. Rev. C **6**, 1705 (1972).
[8] A. E. Antropov, S. I. Vasilev, P. Zurabin, and B. N. Orlov, Izv. Akad. Nauk. SSSR, Ser. Fiz. **38**, 2175 (1974) [Bull. Acad. Sci. USSR, Phys. Ser. **37**, 1873 (1973)].
[9] K. Jankowksi, A. Grzeszczuk, M. Siemanszko, A. Surowiec, W. Zipper, A. Budzanowski, and E. Kozik, Nucl. Phys. **A426**, 1 (1984).
[10] F. Michel, J. Albinski, P. Belery, Th. Delbar, Gh. Grégoire, B. Tasiaux, and G. Reidemeister, Phys. Rev. C **28**, 1904 (1983).
[11] F. Michel, G. Reidemeister, and S. Ohkubo, Phys. Rev. Lett. **57**, 1215 (1986).
[12] F. Schmittroth, W. Tobocman, and A. A. Golestanch, Phys. Rev. C **1**, 377 (1970).
[13] I. Reichstein and F. B. Malik, Phys. Lett. **37B**, 344 (1971).
[14] P. Manngård, M. Brenner, M. M. Alam, I. Reichstein, and F. B. Malik, Nucl. Phys. **A504**, 130 (1989).
[15] A. S. B. Tariq, A. F. M. M. Rahman, S. K. Das, A. S. Mondal, M. A. Uddin, A. K. Basak, H. M. Sen Gupta, and F. B. Malik, Phys. Rev. C **59**, 2558 (1999).
[16] W. Hauser and H. Feshbach, Phys. Rev. **87**, 366 (1952).
[17] S. K. Das, A. K. Basak, K. Banu, A. S. Mondal, A. S. B. Tariq, A. F. M. M. Rahman, H. M. Sen Gupta, and F. B. Malik (unpublished).
[18] M. Yasue, T. Tanabe, S. Kubono, J. Kokame, M. Sugitani, Y. Kadota, Y. Taniguchi, and M. Igarashi, Nucl. Phys. **A391**, 377 (1982).
[19] C. M. Vincent and H. T. Fortune, Phys. Rev. C **2**, 793 (1970).
[20] C. M. Vincent and H. T. Fortune, Phys. Rev. C **7**, 865 (1973).
[21] T. Wada and H. Horiuchi, Phys. Rev. C **38**, 2063 (1988).
[22] T. Wada and H. Horiuchi, Phys. Rev. Lett. **58**, 2190 (1987).
[23] B. Block and F. B. Malik, Phys. Rev. Lett. **19**, 239 (1967).
[24] R. J. Munn, B. Block, and F. B. Malik, Phys. Rev. Lett. **21**, 159 (1968).
[25] K. Bruekner, J. R. Buchler, and M. M. Kelly, Phys. Rev. Lett. **19**, 239 (1967).
[26] F. B. Malik and I. Reichstein, in *Clustering Phenomena in Atoms and Nuclei*, edited by M. Brenner, T. Lönnroth, and F. B. Malik (Springer-Verlag, Berlin, 1992), p. 327.
[27] C. M. Perey and F. G. Perey, At. Data Nucl. Data Tables **17**, 1 (1976).
[28] G. R. Satchler, Nucl. Phys. **55**, 1 (1964).
[29] N. K. Glendenning, in *Nuclear Spectroscopy and Reactions*, edited by J. Cerny (Academic, New York, 1975), Part D, p. 319.
[30] P. D. Kunz, Computer codes DWUCK4, DWUCK5, and CHUCK3 (private communication).
[31] F. G. Perey, in *Proceedings of the Conference on Direct Reactions and Nuclear Reaction Mechanism*, edited by E. Clemental and C. Villi (Gordon and Breach, New York, 1963), p. 125.
[32] F. James and M. Roos, Comput. Phys. Commun. **10**, 343 (1975).
[33] O. Bersillon, Computer code SCAT2, NEA 0829 (private communication).
[34] V. M. Lebedev, A. V. Spassky, I. B. Teplov, L. N. Fateeva, and L. Z. Ismail, Nucl. Phys. **A298**, 206 (1978).
[35] J. M. Barnwell *et al.*, Nucl. Phys. **A388**, 542 (1982).
[36] G. Hauser *et al.*, Nucl. Phys. **A142**, 1 (1972).
[37] P. M. Endt and C. Van der Leun, Nucl. Phys. **A310**, 1 (1978).
[38] P. J. Brussaards and P. W. Glaudemans, *Shell-model Applica-*

tions in Nuclear Spectroscopy (North-Holland, Amsterdam, 1977).
[39] G. R. Satchler, Ann. Phys. (N.Y.) **3**, 275 (1958).
[40] B. Cujec, Phys. Rev. **136**, B1305 (1964).
[41] P. Davidson, *Collective Models of the Nucleus* (Academic, New York, 1968).
[42] H. J. A. De Voigt and B. H. Wildenthal, Nucl. Phys. **A206**, 305 (1973); B. H. Wildenthal and J. B. McGrory, Phys. Rev. C **7**, 714 (1973).
[43] F. B. Malik and W. Scholz, Phys. Rev. **147**, 836 (1966); **150**, 919 (1966); **153**, 1071 (1967).